frontiers | Frontiers in Marine Science

TYPE Original Research
PUBLISHED 11 August 2022
DOI 10.3389/fmars.2022.945908

OPEN ACCESS

EDITED BY
Harald Strauss,
University of Münster, Germany

REVIEWED BY
Aninda Mazumdar,
Council of Scientific and Industrial Research (CSIR), India
Claudio Argentino,
UiT The Arctic University of Norway, Norway

*CORRESPONDENCE
Huiwen Huang
huiwenhuang@scsio.ac.cn

SPECIALTY SECTION
This article was submitted to Marine Biogeochemistry, a section of the journal Frontiers in Marine Science

RECEIVED 17 May 2022
ACCEPTED 19 July 2022
PUBLISHED 11 August 2022

CITATION
Liang Q, Huang H, Sun Y, Gong S, Wang X, Xiao X, Dong Y, Feng J and Feng D (2022) New insights into the archives of redox conditions in seep carbonates from the northern South China Sea.
Front. Mar. Sci. 9:945908.
doi: 10.3389/fmars.2022.945908

New insights into the archives of redox conditions in seep carbonates from the northern South China Sea

Qianyong Liang[1,2,3], Huiwen Huang[1,4]*, Yuedong Sun[1,4], Shanggui Gong[5], Xudong Wang[5], Xi Xiao[1,2,3], Yifei Dong[1,2,3], Junxi Feng[1,2,3] and Dong Feng[5]

[1]Southern Marine Science and Engineering Guangdong Laboratory (Guangzhou), Guangzhou, China, [2]National Engineering Research Center of Gas Hydrate Exploration and Development, Guangzhou, China, [3]MLR Key Laboratory of Marine Mineral Resources, Guangzhou Marine Geological Survey, China Geological Survey, Guangzhou, China, [4]Key Laboratory of Ocean and Marginal Sea Geology, South China Sea Institute of Oceanology, Innovation Academy of South China Sea Ecology and Environmental Engineering, Chinese Academy of Sciences, Guangzhou, China, [5]Shanghai Engineering Research Center of Hadal Science and Technology, College of Marine Sciences, Shanghai Ocean University, Shanghai, China

Modern cold seeps are of fluctuant flux, which could result in variabilities of geochemical archives through intensively influencing the redox condition in pore fluids. However, the geochemical archives are not fully understood when the redox condition changes. Here, tubular carbonates from the Shenhu Sea Area were used to reconstruct the formation environment and redox conditions. The moderately negative $\delta^{13}C$ values of the carbonates (–40.1‰ to –30.8‰, VPDB) indicate a mixed carbon source of thermogenic and biogenic methane. The low $\delta^{18}O$ values (–2.7‰ to 1.0‰, VPDB) suggest a type of ^{18}O-depleted pore fluid possibly influenced by gas hydrate formation. Co-variation of Mo_{EF}, W_{EF}, Co_{EF}, and Cr_{EF} suggests that high Fe contents in the rims of samples R1 and R2 are induced by Fe (oxyhydr)oxidation enrichment, while the positive correlation between Mo_{EF} and Mn/Al ratio indicates that high Mn contents in the rims of samples R3 and R4 are induced by Mn (oxyhydr) oxidation enrichment. The occurrence of Fe or Mn enrichment in the rims and the absence of Fe/Mn enrichment in the cores suggest Fe/Mn (oxyhydr)oxides forming in pore fluid rather than in bottom seawater. The carbonate phases of the rims enriched in Fe (oxyhydr)oxides are dominated by high magnesium calcite, while those of the rims enriched in Mn (oxyhydr)oxides are dominated by aragonite. The occurrence of Fe or Mn (oxyhydr)oxides corresponds to the previously proposed formation depth for the carbonate phase. The occurrence of dissolution textures in these rims indicates episodic oxic conditions, which would facilitate Fe^{2+}/Mn^{2+} oxidation. We suppose that the Fe^{2+} and Mn^{2+} could be supplied through fluid seepage or diffusion from underlying sediments when the flux decreased. Similar archives may be applied to qualitatively reflect the

changes of redox conditions in seep systems. Similar scenarios may help us understand the geochemical records in seeps of fluctuant flux.

KEYWORDS

redox condition, Fe/Mn oxidation, seep intensity, cold seep, tubular carbonates

Introduction

Methane, existing as free gas, dissolved gas, or gas hydrate in marine sediments, is a powerful greenhouse gas (Milkov, 2004). Nowadays, methane seeps are limited at scattered spots on the marginal seafloor (Tryon et al., 1999; Campbell, 2006; Klaucke et al., 2010; Suess, 2018). Variable seepage flux results in significant differences in chemical and physical conditions at the seafloor (Tryon et al., 1999; Luff and Wallmann, 2003; Solomon et al., 2008; Peckmann et al., 2009; Hu et al., 2014; Li et al., 2021). Only methane in vigorous seeps can escape from the subsurface sediment (Knab et al., 2009) and is consumed by aerobic oxidation of methane in bottom seawater (Tavormina et al., 2008). During some geologic periods, methane seeps could be more intensive and pervasive, possibly changing the geochemical composition and redox condition of seawater and even elevating the greenhouse effect (Paull et al., 1991; Dickens et al., 1995; Kennett et al., 2000; Schrag et al., 2002; Boetius and Wenzhöfer, 2013; Ruppel and Kessler, 2017). Consequently, increasing attention has been paid to the archives of the seepage environment and seepage intensity in modern and ancient seep systems (e.g., Peckmann et al., 2009; Clark et al., 2010; Hu et al., 2014; Lu et al., 2017; Li et al., 2021).

Today, an estimated 90% of the seep methane is consumed by anaerobic oxidation of methane mainly coupled with sulfate reduction (SR-AOM, Equation 1) in marine sediments (Boetius et al., 2000; Knittel and Boetius, 2009). The reaction of SR-AOM is mediated by a consortium of methanotrophic archaea and sulfate-reducing bacteria mainly at the sulfate–methane transition zone (SMTZ) where methane and sulfate are exhausted (Hinrichs et al., 1999; Boetius et al., 2000; Jørgensen et al., 2004). Due to the production of HCO_3^-, alkalinity increases locally in pore fluid, facilitating precipitation of authigenic carbonates (Equation 2) in the shallow subsurface (e.g., Hovland et al., 1987; Aloisi et al., 2000; Reitner et al., 2005). Due to their direct relationship to the process of AOM, seep carbonates served as excellent records of seep activities (e.g., Peckmann et al., 2001; Peckmann et al., 2009; Feng et al., 2009; Feng et al., 2016; Argentino et al., 2019).

$$CH_4 + SO_4^{2-} \rightarrow HS^- + HCO_3^- + H_2O \quad (1)$$

$$HCO_3^- + Ca^{2+} \rightarrow CaCO_3 + H^+ \quad (2)$$

The changes in geochemical composition and redox condition in pore water influenced by the fluctuation of seep intensity result in variable archives in authigenic carbonates (Lapham et al., 2008; Solomon et al., 2008; Feng et al., 2009; Zwicker et al., 2015). Variation of Ce anomaly, Mo enrichment factors, and molecular fossils were used as indicators of redox conditions during carbonate formation, allowing for a better understanding of the variations in porewater component and seep intensity (Feng et al., 2009; Birgel et al., 2011; Hu et al., 2014). Ce^{3+} would be oxidized to Ce^{4+} and eliminated from seawater under oxic conditions, resulting in Ce anomaly being widely used as a proxy for redox condition (e.g., Feng et al., 2009; Birgel et al., 2011; Hu et al., 2014; Wei et al., 2020). Negative Ce anomalies of carbonates reflect oxic conditions, while positive Ce anomalies reflect reducing conditions (Feng et al., 2009; Wei et al., 2020). In oxic seawater, molybdate (MoO_4^{2-}) is the dominant molybdenum species (Helz et al., 2022), which is mainly sequestered by Mn and Fe (oxyhydr)oxides (Phillips and Xu, 2021). In reducing pore fluids, MoO_4^{2-} converts into thiomolybdate species ($MoO_xS_{4-x}^{2-}$) *via* stepwise replacement of the oxygen atoms in molybdate by sulfur atoms under sufficiently sulfidic conditions (Phillips and Xu, 2021 and references therein). Thiomolybdate then reacts with either Fe sulfides through thiomolybdate–Fe sulfide interactions or organic matter (OM) through Mo–OM interactions, resulting in Mo enrichment in sediments (Helz et al., 1996; Helz et al., 2011). Accordingly, real negative Ce anomaly, the absence of Mo enrichment, and the occurrence of lipid biomarkers for aerobic methanotrophic bacteria suggested that temporary oxic conditions prevailed during carbonate precipitation (Feng et al., 2009; Birgel et al., 2011; Hu et al., 2014). These studies emphasized the redox condition changes during the carbonate precipitating when seep flux fluctuates, providing a thinking direction for the geochemical records of seepage intensity (Hu et al., 2014). Accompanied with seep methane, Fe^{2+} and Mn^{2+} could also migrate to the near subsurface from underlying sediments (Bayon et al., 2011; Hu et al., 2014). The autochthonous-origin Fe/Mn has been recognized in the

sediments of Lake Baikal, which might serve as proxy indicators for redox conditions (Granina et al., 2004). In a seepage system, a decrease in seepage flux could induce a downward migration of redox zones in marine sediments, possibly resulting in seepage Fe^{2+} and Mn^{2+} oxidation in the setting where carbonate precipitated before. Such a combination of the autochthonous-origin Fe/Mn (oxyhydr)oxide and carbonates could serve as the archive of redox conditions and seepage intensity in methane seeps. However, such scenarios have not yet been recognized in seep systems.

Here, the redox condition and formation environment were reconstructed by redox-sensitive elements of five tubular carbonates from the Shenhu Sea Area on the northern slope of the South China Sea. It was suggested that tubular carbonates form when seepage flux is intensive or at least highly focused (Stakes et al., 1999; Jin et al., 2021). For instance, Oppo et al. (2015) suggested that tubular carbonates act as focused SMTZ in the sulfate-rich pore fluid in sediments. Our results illustrate that tubular carbonates record changes in redox conditions between suboxic–anoxic and temporarily oxic conditions when flux fluctuates in vigorous seeps. This study explores our understanding of geochemical records in seep carbonates and sheds light on its application in redox-sensitive elements in further studies in ancient seep carbonates.

Geological setting and sampling

The carbonates were recovered during the *Haiyang-4* cruise using bottom trawlers by the Guangzhou Marine Geological Survey in 2017 from the Shenhu Sea Area in the South China Sea. The South China Sea is located at the junction of the southeastern Eurasian, western Pacific oceans, and northern Indo-Australian plates. The Shenhu Sea Area is located on the northern continental slope of the South China Sea (Figure S1). In this area, the water depth is between 800 and 2,000 m (Liu et al., 2012). Bottom-simulating reflectors have been widely recognized in the Shenhu Sea Area at about 150 to 350 m below the seafloor, reflecting the accumulation of gas hydrates in buried sediments (Wu et al., 2008; Wang et al., 2018). The burial of gas hydrate was confirmed during a drilling investigation of gas hydrate in 2007 (Zhang et al., 2007). Gas chimneys and faults, which are supposed to be the important fluid migration pathways for methane, were also widely recognized in sediments in Shenhu Sea Area (Wu et al., 2011; Yang et al., 2017; Wang et al., 2018). The gas chimneys extend more than 1,000 ms TWT (two-way travel time) deep, suggesting that methane in gas hydrate was migrated from deeply buried methane (Yang et al., 2017). Nowadays, active cold seeps are absent in the Shenhu Sea Area, and the methane flux is minor (Wu et al., 2011; Feng et al., 2018). However, the discovery of seep carbonates, especially tubular carbonates, indicates intensive methane seepage in this area before.

Methods

The carbonates were washed and air-dried on board. They were cut in suitable directions according to the different morphology. Most carbonate conduits were cut at cross-sections, while sample R1 was cut at the vertical section due to its small size. Subsamples were micro-drilled from the resultant fresh sections. Thin sections were observed with a LEICA-DMRX optical microscope at the South China Sea Institute of Oceanography, Chinese Academy of Sciences. Photographs were pictured using the Leica QWin software (Version V2.6, Leica Microsystems Imaging Solutions Ltd., Cambridge, UK).

The subsamples were micro-drilled from the fresh-cut surface and crushed into powders (<200 mesh) for mineralogical analysis. Mineralogical measurements were performed using a D8 ADVANCE X-ray diffractometer at the South China Sea Institute of Oceanology, Chinese Academy of Sciences. The X-ray was generated by a copper Kα tube radiation at 40 kV and 40 mA. Scan angles are between 5° and 65° (2θ) with an angle step of 0.02° and a counting time of 0.15 s per step. Diverging, scattering, and receiving slits were 0.5°, 0.5°, and 0.15 mm, respectively. The $MgCO_3$ content of carbonate minerals was calculated using the position of the (104) peak (Goldsmith et al., 1961).

Carbon and oxygen isotope compositions of carbonate conduits were determined at the Third Institute of Oceanography, State Oceanic Administration. About 100-μg powders were treated with 100% phosphoric acid at 70°C to release CO_2 gas. The extracted and purified gas were introduced into a GasbenchII-Delta V Advantage mass spectrometer. The data were calibrated with IAEA-NBS-18 and IAEA-CO-8 standards. The carbon and oxygen stable isotope compositions were reported in δ notation per mil (‰) relative to the Vienna Pee Dee Belemnite (VPDB) standard. The $\delta^{13}C$ and $\delta^{18}O$ reproducibility were ±0.20‰ and ±0.20‰, respectively.

The preparation for the major and trace element analyses follows Hu et al. (2014). About 20 mg of bulk samples for major and trace element analyses were treated with hydrofluoric acid/nitric acid solutions. Major and trace element analyses were conducted with an iCAP 7200 ICP-AES (Thermo Fisher, USA) and an iCAPQ ICP-MS (Thermo Fisher, USA) at the Third Institute of Oceanography, Ministry of Natural Resources. Enrichment factors (EF) were calculated to compare the enrichment of each trace metal in the carbonates ($X_{EF} = [(X/Al)_{sample}/(X/Al)_{reference}]$, where "X" and "Al" denote the contents of elements X and Al. The post-Archean Australian shale (PAAS) compositions (Taylor and McLennan, 1985) or the Earth's upper crust composition (McLennan, 2001) was used as "Reference." It is suggested that X_{EF} >3 reflects a detectable enrichment and X_{EF} >10 represents a moderate to strong enrichment (Algeo and Tribovillard, 2009).

The Fe and Mn distributions in the fresh-cut surface of sample R3 were determined by μXRF geochemical maps using a Bruker Tornado μXRF (M4 Plus) at the Guangzhou Tuoyan Testing Technology Co., Ltd., in Guangzhou, China. The analysis condition is 50 kV of acceleration voltage and 300 μA of electric current. The spot size is 25 μm and the dwell time is 5 ms per pixel with two frame counts. The Bruker M4 Tornado software was used to process raw data, analyze spectral peak information, and export element distribution maps.

Results

Petrography and mineralogy

All the tubular carbonates have a 1–5-cm-thick rim (Figure 1), while the central conduits of samples R2, R3, and R5 are partially infilled. The fresh-cut surface of the carbonates is terra brown to light gray. The outer and inner surfaces of the carbonates are coated by Fe/Mn (oxyhydr)oxides, reflecting secondary oxidation

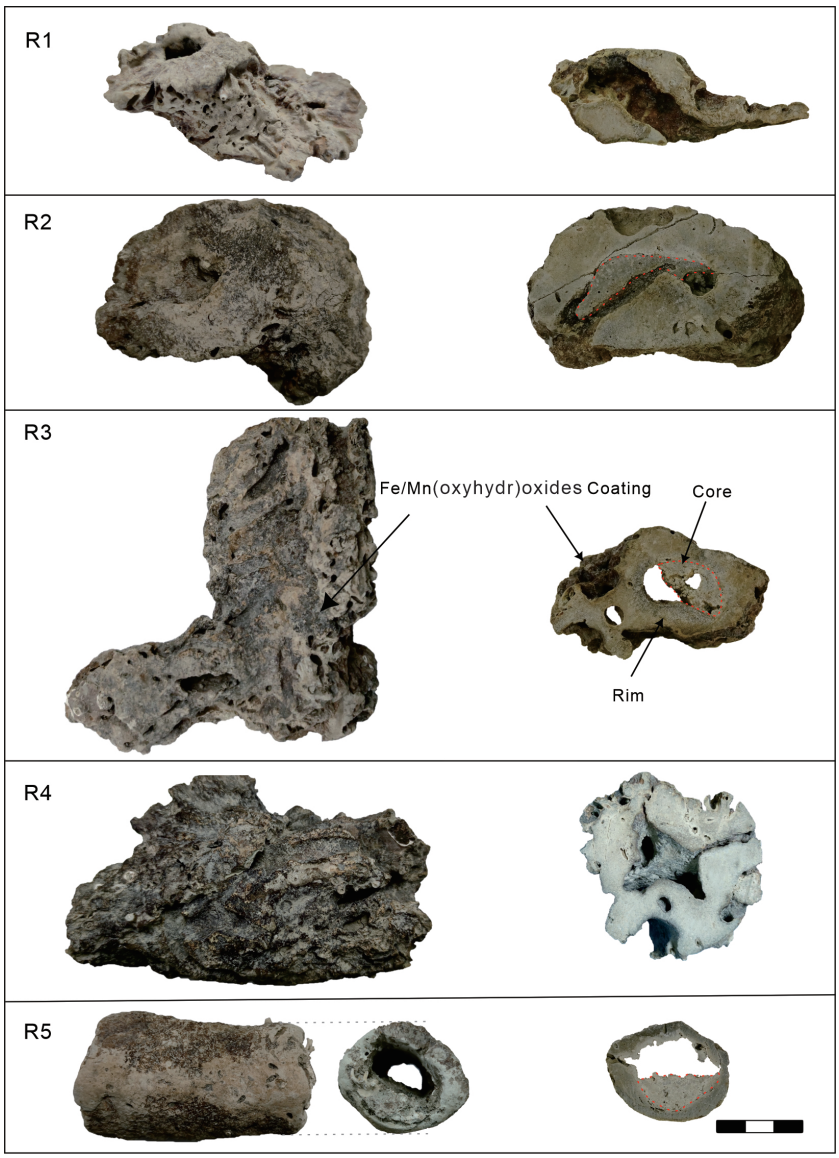

FIGURE 1
Morphologies of the selected tubular carbonates (left) and their fresh-cut surface (right) in this study. The cores were circled by red dashed lines. The scale bar is 3 cm.

precipitation on the sample surface during exposure to bottom seawater after precipitation. The holes on the outer surface represent boring by marine mollusks at seeps, suggesting the carbonates precipitated in the shallow subsurface. The carbonates are mostly microcrystalline. Detrital minerals, pyrite, and bioclasts are cemented by microcrystalline carbonates (Figure 2). Dissolution of bioclasts and grains can be recognized in the rims of samples R1, R2, R3, and R4 (Figure 2C).

The carbonate contents range from 51.9% to 91.2%. The major mineral of carbonate phases was illustrated by the plots of Mg/Ca versus Sr/Ca (Figure 3 modified after Bayon et al., 2007). To verify the results illustrated by the Mg/Ca–Sr/Ca diagram, five subsamples were determined by an X-ray diffractometer (Figure S2). The rims of samples R1, R2, and R5 are mainly composed of high magnesium calcite (HMC), while those of samples R3 and R4 are mainly composed of aragonite. The infilled cores in samples R2, R3, and R5 are mainly composed of aragonite.

Stable carbon and oxygen isotopic composition

The carbon and oxygen isotope compositions are shown in Table S1 and Figure 4. The oxygen isotope compositions range from −2.7‰ to 1‰ (average = −1.1‰). The $\delta^{18}O$ values of the carbonates mainly composed of aragonite vary from −1.8‰ to 1.0‰ (average = −0.6‰), which is higher than those of the carbonates mainly composed of HMC (−2.7‰ to −0.8‰, average = −1.7‰). Such discrepancy is largely induced by the difference in oxygen isotope fractionation during carbonate precipitation. The $\delta^{13}C$ values of the carbonates range between −40.1‰ and −30.5‰ (average = −34.1‰). The carbonates mainly composed of aragonite reveal relatively lower $\delta^{13}C$ values (subsamples R2-5 and R5-3, samples R3 and R4), ranging from −40.1‰ to −33.8‰ (average = −36.3‰) than those mainly composed of HMC, of which $\delta^{13}C$ values range from −32.8‰ to −30.8‰ (average = −31.8‰).

Major and trace elements

The major element contents are shown in Table S2. The rims mainly composed of HMC yield relatively higher Al_2O_3 and Fe_2O_3 contents (Al_2O_3: 4.96% to 6.18%, average = 5.37%; Fe_2O_3: 2.00% to 3.76%, average = 2.88%). Among these HMCs, the rim of sample R5 reveals the lowest Fe_2O_3 (2.00% to 2.32%, average = 2.15%). In contrast, the rims mainly composed of aragonite yield lower contents of Al_2O_3 and Fe_2O_3 (Al_2O_3: 3.46% to 5.19%, average = 4.03%; Fe_2O_3: 1.42% to 2.66%, average = 1.79%).

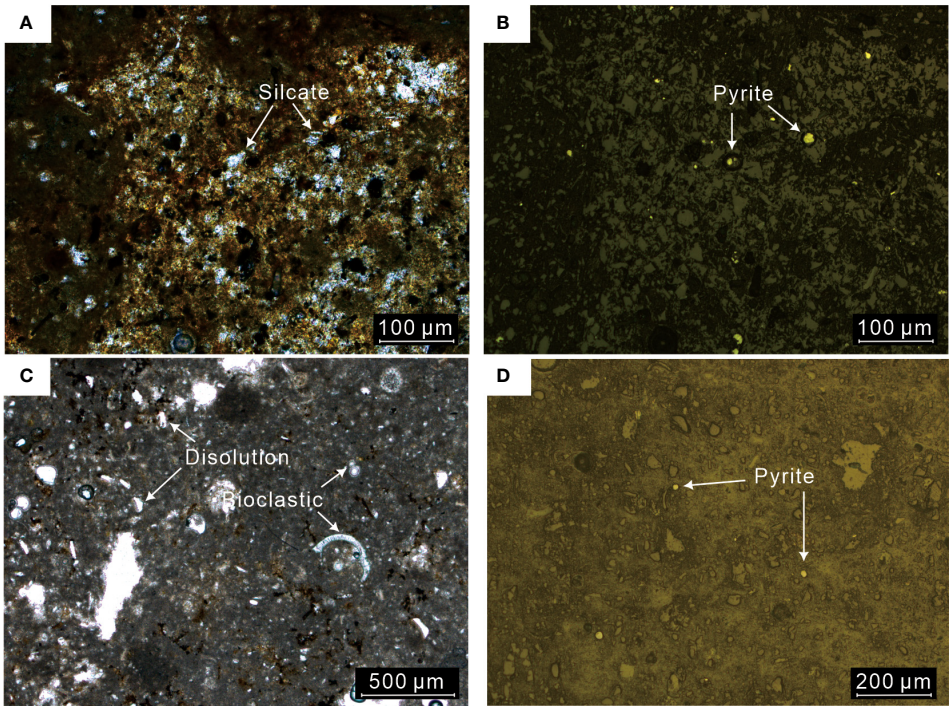

FIGURE 2
Thin section photomicrographs of carbonates R1 **(A, B)** and R4 **(C, D)**. **(A, C)** Under plane-polarized light; **(B, D)** under reflected light.

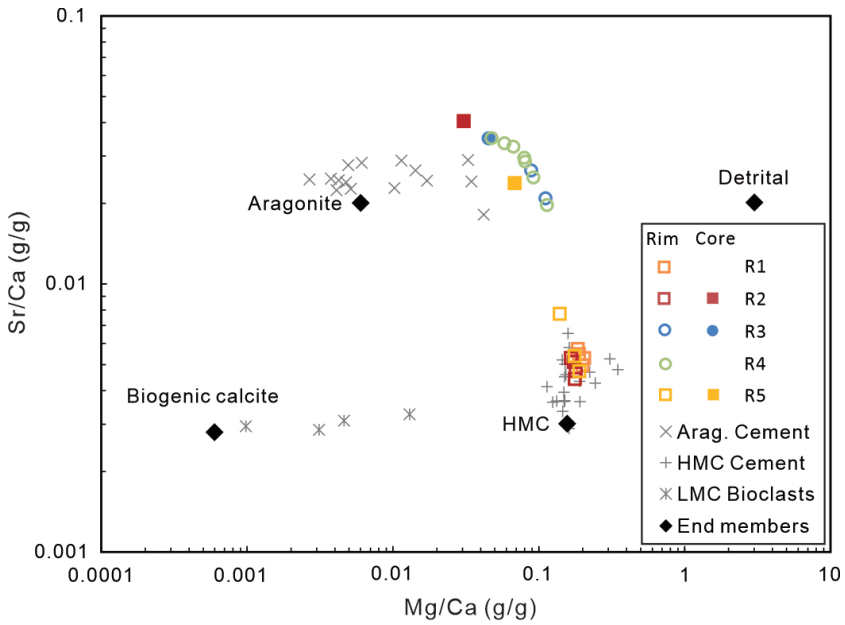

FIGURE 3
The relationship of Sr/Ca (g/g) vs. Mg/Ca (g/g) ratios reflects the composition of the mineral of the studied carbonates. The results of aragonite cement, HMC cement, and low magnesium calcite (LMC) reported by Joseph et al. (2013) are for comparison. The end members of Sr/Ca and Mg/Ca ratios of HMC, aragonite (Gong et al., 2018), and bioclastic and detrital fraction (Yang et al., 2014) are denoted in black rhombus.

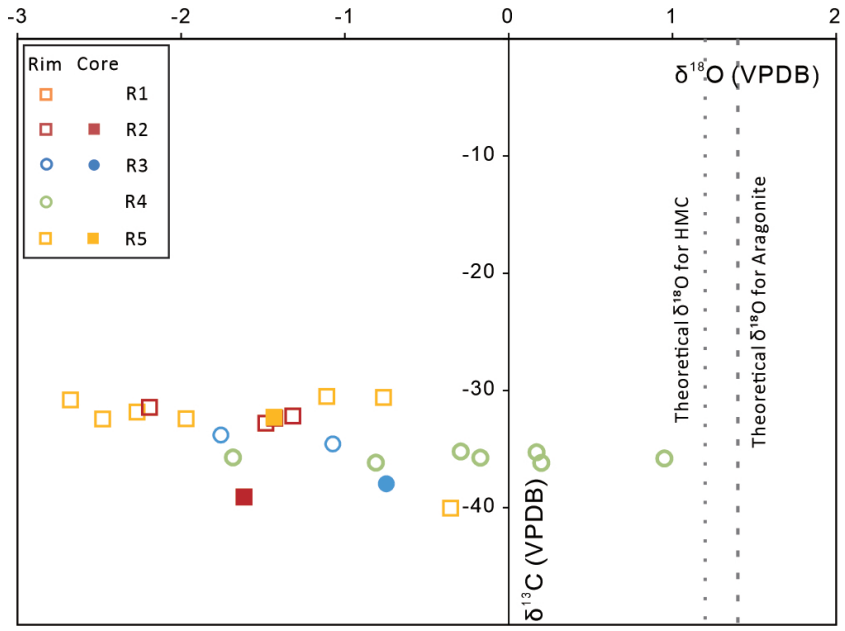

FIGURE 4
Plots of $\delta^{13}C$ and $\delta^{18}O$ values of the tubular carbonates. Dashed lines represent the theoretical $\delta^{18}O$ values of authigenic HMC (10 mol% $MgCO_3$) and aragonite in equilibrium with modern bottom seawater [$\delta^{18}O$ value = 0‰ (V-SMOW); temperature = 10.8°C (Tong et al., 2013)].

Similar to the aragonite rims, the cores of the tubular carbonates yield low Al_2O_3 and Fe_2O_3 contents (Al_2O_3: 2.05% to 3.41%, average = 2.85%; Fe_2O_3: 0.76% to 1.61%, average = 1.32%).

The trace element contents of the bulk carbonates are listed in Table S3, and their enrichment factors or X/Al ("X" and "Al" denote the contents of elements X and Al) are shown in Table S4. Manganese contents of the carbonates are highly variable between 160 and 5,464 ppm. The rims composed of aragonite reveal high Mn contents (2,199 to 5,464 ppm, average = 3,483 ppm). The rims composed of HMC reveal moderate Mn contents, ranging from 224 to 1,779 ppm (average = 858 ppm), among which sample R5 yields the lowest Mn content ranging from 224 to 1,323 ppm (average = 671 ppm). The infilled cores of the tubular carbonates reveal the lowest Mn contents (160 to 747 ppm, average = 365 ppm), which is close to those of sample R5. It should be noted that the Mn and Fe contents of the rim of each carbonate do not show any regular distribution characteristics, suggesting that the Mn and Fe phase was cemented in the carbonates. The rims of carbonates R1 and R2 yield higher molybdenum contents (40.1 to 194.9 ppm, average = 87.0 ppm) and lower U contents (2.44 to 3.51 ppm, average = 2.89 ppm). In contrast, the rims of sample R5 and the subsamples composed of aragonite reveal low Mo contents (0.33 to 6.38 ppm, average = 2.67 ppm) and higher U contents (3.29 to 7.68 ppm, average = 5.31 ppm). According to the contents of Fe, Mn, and Mo in the subsamples, we divided the subsamples into three groups. The rims of samples R1 and R2 mainly composed of HMC (group 1) reveal high Fe and Mo content. The rims of samples R3 and R4 that are mainly composed of aragonite (group 2) reveal high Mn content and moderate Mo enrichment. The rims of sample R5 and the cores of samples R2, R3, and R5 (group 3: sample R5 and cores) yield relatively low Fe, Mn, and Mo contents.

Discussion

Tubular carbonates precipitate at methane seeps

Tubular carbonates are common in many modern and ancient cold seeps worldwide, such as the northern South China Sea, the Mediterranean Sea, the Campos Basin (offshore Brazil), the Krishna–Godavari Basin (offshore India), the Enza River field in Northern Apennines in Italy, and the Hikurangi Margin in New Zealand (e.g., Campbell et al., 2008; Mazumdar et al., 2009; Mazumdar et al., 2011; Wirsig et al., 2012; Bayon et al., 2013; Joshi et al., 2014; Oppo et al., 2015; Yang et al., 2018). Their precipitation is attributed to increasing alkalinity during methane oxidation mainly driven by sulfate reduction. The negative $\delta^{13}C$ values of the studied carbonates ranging from −40.1‰ to −30.5‰ suggest that the seep methane is of a mixed origin (cf. Peckmann and Thiel, 2004). Wei et al. (2018) have analyzed the gas composition (C1/(C2+C3)), carbon, and hydrogen isotope composition of hydrate-bound gas in the buried sediment in the Shenhu Sea Area. The results indicate a mix of methane originating from mainly thermogenic sources with a certain proportion of biogenic sources (Wei et al., 2018), supporting our proposal.

The oxygen isotopic composition of authigenic carbonates is a function of the oxygen isotopic composition of the parent fluid, mineralogy, and formation temperature, providing a useful tool to reconstruct the ambient temperature and fluid origin in which authigenic carbonates precipitate (e.g., Naehr et al., 2000; Greinert et al., 2013). Assuming that the studied carbonates precipitated from modern bottom seawater in the Shenhu Sea area, with a $\delta^{18}O$ value of 0‰ (V-SMOW) at a temperature of 10.8°C (Tong et al., 2013), theoretical $\delta^{18}O$ values of the carbonates can be calculated using the equilibrium formula for calcite (Kim and O'Neil, 1997) and aragonite (Kim et al., 2007). To simplify the calculation, HMC of 10% mol $MgCO_3$ was used in this study for the correction by +0.06‰ per mol% $MgCO_3$ (Tarutani et al., 1969). The theoretical $\delta^{18}O$ values are 1.2‰ for HMC and 1.4‰ for aragonite. Compared to the calculated values, the $\delta^{18}O$ values of the studied carbonates are lower, while those of the previously reported carbonates in the Shenhu area ($\delta^{18}O$ = 1.4‰ to 4.2‰, VPDB) are comparable or higher (Tong et al., 2013). Considering that massive gas hydrate is buried in the underlying sediments, the obvious fluctuation of the temperature of seep fluids is excluded. The change of oxygen isotope composition of pore fluid most likely induced such differences in $\delta^{18}O$ values of authigenic carbonates. Due to the deep-water depth and significant distance to the shore, freshwater or evaporated seawater is out of consideration. Previously, the formation and dissolution of gas hydrate have been suggested to attribute to the formation of ^{18}O-depleted and ^{18}O-rich fluid in seepage systems, respectively (e.g., Bohrmann et al., 1998; Aloisi et al., 2000; Tong et al., 2013). As gas hydrate is forming, it would prefer ^{18}O rather than ^{16}O, producing ^{18}O-depleted residual fluid. During gas hydrate dissolution, ^{18}O-rich water is released into the pore fluid, increasing its $\delta^{18}O$ value. Consequently, Tong et al. (2013) suggested that the high $\delta^{18}O$ values of seep carbonates in the Shenhu Sea Area could be induced by the dissolution of gas hydrate. Similarly, the low $\delta^{18}O$ values of our studied carbonates could be related to gas hydrate formation. The various $\delta^{18}O$ values of carbonates collected in the same area could reflect fluctuations in the stability of buried gas hydrate.

Fe/Mn (oxyhydr)oxide in the rims of tubular carbonates

Sample R5 and the cores of the tubular carbonates (group 3 hereafter) reveal mild Mn, Fe, and Mo enrichments. The elemental features are comparable to those of the carbonates precipitated under suboxic to anoxic conditions (cf. Hu et al., 2014). Mo_{EF} and U_{EF} of the subsamples plot close to the suboxic

to anoxic zone, favoring that sample R5 and the cores of the tubular carbonates precipitated under suboxic to anoxic conditions (Figure 5).

The HMC rims of carbonates R1 and R2 (group 1 hereafter) yielded higher Fe/Al ratios (0.65 to 0.91) than those of other subsamples in this study (0.47 to 0.65) and the surface sediments in the Shenhu area (Fe/Al = 0.52, Zhao et al., 2009). Such Fe enrichment could be induced by precipitation of pyrite or Fe (oxyhydr)oxides. Framboidal pyrites, which are induced by the production of H_2S during sulfate reduction (Peckmann and Thiel, 2004), are common in our studied carbonates. Significant Mo enrichment is recognized in group 1 (Figure 6). Previous studies attributed high Mo contents in seep sediments and methane-derived carbonates to sulfidic conditions produced by SR-AOM (Sato et al., 2012; Hu et al., 2014; Lin et al., 2021). Mo content in the sediments rarely exceeds 25 ppm when sulfidic conditions are restricted to porewaters, while Mo content exceeds 60 ppm and even over 100 ppm in the sediments where hydrogen sulfide is present in bottom seawater (Scott and Lyons, 2012). Accordingly, Hu et al. (2014) proposed that the significantly high Mo content in seep carbonates could reflect a situation when hydrogen sulfide is present in the seawater column. However, high Mo and low U of group 1 result in Mo_{EF} and U_{EF} values plot close to Fe–Mn shuttle zones in the Mo_{EF}–U_{EF} diagram (Figure 5; modified after Algeo et al., 2009). The scenario indicates an intensive influence of Fe or Mn (oxyhydr)oxides. Additionally, the enrichment factors of W, Co, and Cr elements in group 1 show positive correlations with Mo_{EF} (Figure 7). Tungsten, Co, and Cr elements can form strong surface complexes on Fe/Mn (oxyhydr)oxides (e.g., Gustafsson, 2003; Smrzka et al., 2019; Akintomide et al., 2021). Among these elements, Co and Cr do not co-precipitate with Fe sulfides due to their slow reaction with dissolved sulfide, while only W can co-precipitate with pyrite at sulfidic conditions (Smrzka et al., 2019). Consequently, Fe enrichment in group 1 can be, at least partially, attributed to the precipitation of Fe (oxyhydr)oxides.

On the contrary, the aragonite rims of carbonates R3 and R4 (group 2 hereafter) reveal significant Mn enrichment rather than high Fe contents (Figure 6). Compared to group 1 and group 3, these subsamples reveal moderate Mo enrichment. Mo_{EF} of group 2 shows a positive correlation with Mn/Al (Figure 7). The Mo/Mn ratios of group 2 (~0.001) are much lower than those of group 1 with high Mo content (~0.104) and are close to the proposed constant Mo/Mn weight ratio of about 0.002 in sediments underlying oxic bottom waters in the Santa Cruz Basin (Shaw et al., 1990), where Mo recycled with Mn (oxyhydr) oxide. Consequently, Mn enrichment of group 2 is attributed to high Mn (oxyhydr)oxide content.

Episodic oxic condition during methane seepage

Due to exposure to bottom seawater after formation, the outer and inner surfaces of the tubular carbonates are rich in Fe/Mn

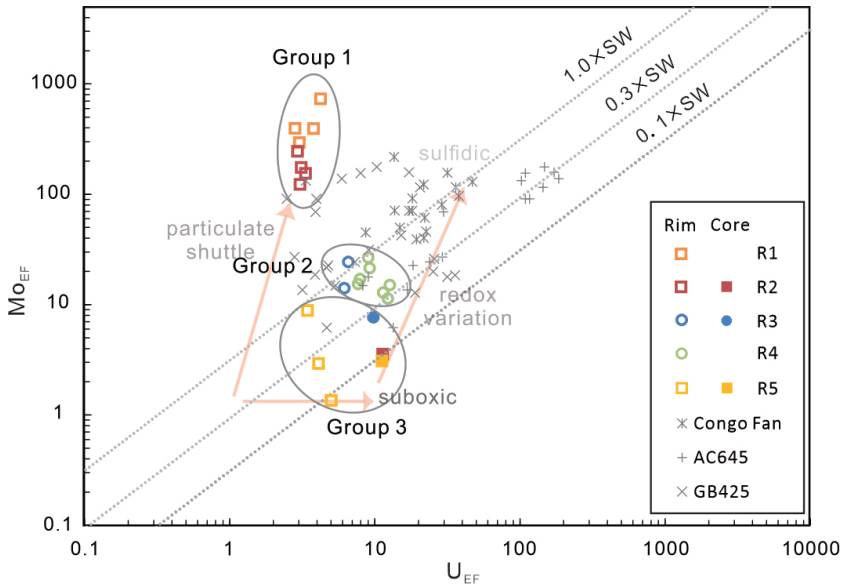

FIGURE 5
Plots of Mo_{EF} vs. U_{EF} for the studied authigenic carbonates (modified from Hu et al., 2014). The results of the artificially divided groups in this study were circled in gray. Enrichment factors of Mo and U are calculated by being normalized to the post-Archean Australian shale (PAAS) composition (Taylor and McLennan, 1985).

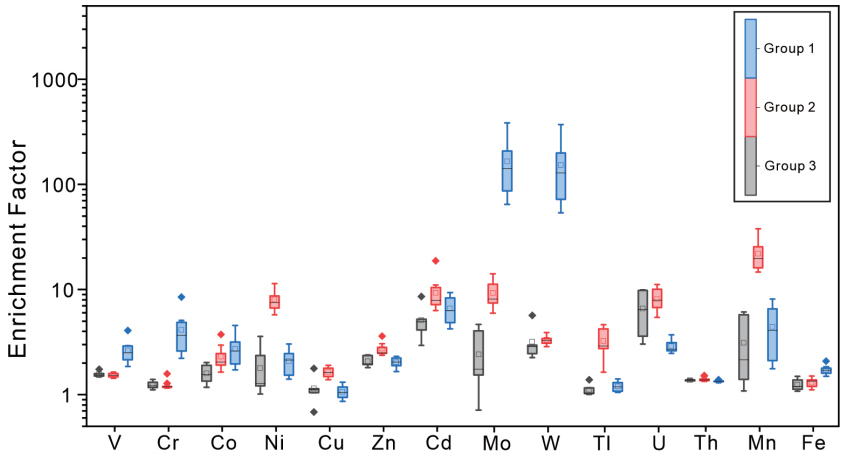

FIGURE 6
Enrichment patterns of trace elements in seep carbonates relative to the Earth's upper crust compositions (McLennan, 2001). Box plots show the maximum value, minimum value, median value, interquartile range, and outliers for group 1 (HMC rims of samples R1 and R2), group 2 (aragonite rims of samples R3 and R4), and group 3 (sample R5 and cores of the tubular carbonates).

(oxyhydr)oxides. However, two factors indicate that Fe/Mn (oxyhydr)oxides in the tubular carbonates were deposits from pore fluid rather than being products of the coating during the carbonate's exposure. 1) The adhering Fe/Mn (oxyhydr)oxides on the inner and outer surfaces are both enriched in Fe and Mn (Figure 7), while group 1 is rich in Fe and group 2 is rich in Mn, respectively. 2) Regardless of the high Fe or Mn contents in the rims (Figure 8), the cores in samples R2 (one of the tubular carbonates with an HMC rim) and R3 (one of the tubular carbonates with an aragonite rim) show neither Fe nor Mn enrichment.

Significantly elevated Fe^{2+} and Mn^{2+} concentrations in pore fluid could be produced by Fe/Mn reduction in reducing settings

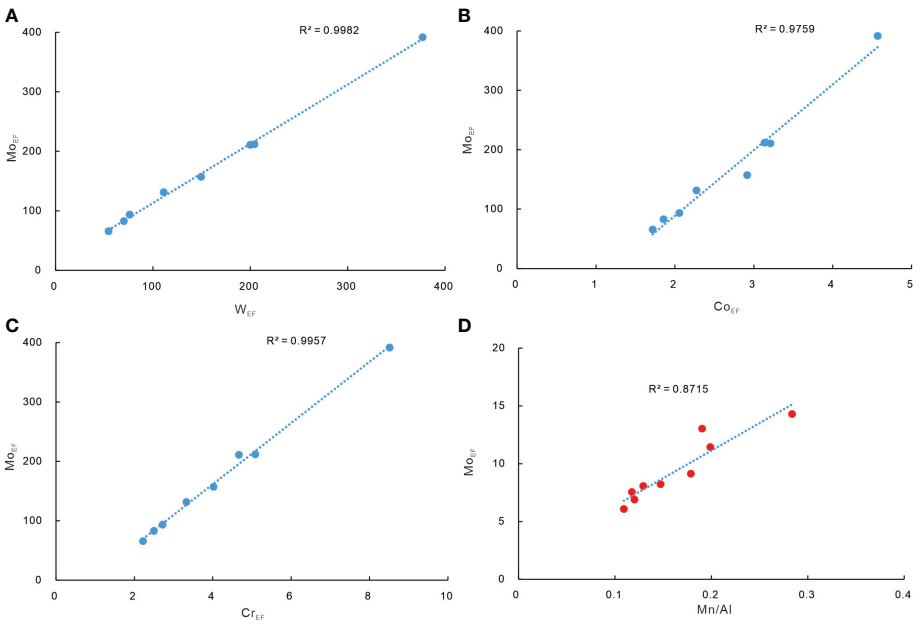

FIGURE 7
The Mo_{EF} of the HMC rims of samples R1 and R2 shows a positive correlation with W_{EF} **(A)**, Co_{EF} **(B)**, and Cr_{EF} **(C)**. **(D)** Mo_{EF} and Mn/Al of the aragonite rims of samples R3 and R4 yield a positive correlation.

(Schulz, 2006). These ions would migrate upward to the sediment subsurface through fluid seepage or diffusion from underlying reducing settings (e.g., Bayon et al., 2011) and precipitate Fe/Mn (oxyhydr)oxides under oxic conditions (cf. Bayon et al., 2011; Hu et al., 2014). Schulz (2006) suggests that the reaction could occur several centimeters below the sediment surface. For instance, elevated Fe/Mn contents in the sediments of Lake Baikal are supposed to result from Fe^{2+}/Mn^{2+} oxidation (Granina et al., 2004). It is suggested that oxic conditions in pore fluid favor carbonate dissolution rather than precipitation (Cai et al., 2006). Dissolution of carbonate minerals in seep carbonates is believed to be caused by increased pCO_2 and decreased pH, which is induced by aerobic oxidation of methane and H_2S (Matsumoto, 1990; Cai et al., 2006; Himmler et al., 2011; Feng et al., 2014). Dissolution texture in these rims of the carbonates favors the proposal of episodic oxic conditions in pore fluid, satisfying the condition for oxidation of Fe^{2+} and Mn^{2+} (cf. Cai et al., 2006; Schulz, 2006). Group 1 with Fe (oxyhydr)oxide enrichment is mainly composed of HMC, and group 2 with Mn (oxyhydr)oxide enrichment is mainly composed of aragonite. The zone of iron reduction is situated below the Mn reduction zone in marine sediments (Schulz, 2006; Smrzka et al., 2019; Smrzka et al., 2020). The presence of Fe (oxyhydr)oxide enrichment in group 1 and Mn (oxyhydr)oxide enrichment in group 2 corresponds to the proposal that HMC precipitates in deeper sediments and aragonite precipitates at a shallower depth (e.g., Feng et al., 2009; Greinert et al., 2013). Consequently, we suggest that Fe/Mn (oxyhydr)oxides in the rims of the tubular carbonates precipitate through oxidation of Fe^{2+} or Mn^{2+} in pore fluid when fluctuating seepage created episodic oxic conditions.

Tong et al. (2013) suggested that the rim of a seep tubular carbonate from the Shenhu Sea Area is about 170 ka older than its core. The seep conduit existed for a long time in shallow sediments after the rim of tubular carbonate precipitation. As for our studied carbonates, the long-existing conduits may facilitate oxic seawater entering the rims through the hollow tube when seep flux is slow, forming a condition for Fe^{2+} or Mn^{2+} precipitation (Figure 9). Actually, an inner zone with high Mn content and an outer zone with slightly higher Fe content are recognized in the rim of sample R3 which is mainly composed of aragonite (Figure 8), suggesting that electric potential decreased from the inside out. Once the seep flux increased again, the carbonate core would precipitate and partially infill the conduit of the tubular carbonate under reductive conditions. In this situation, the rims of the tubular

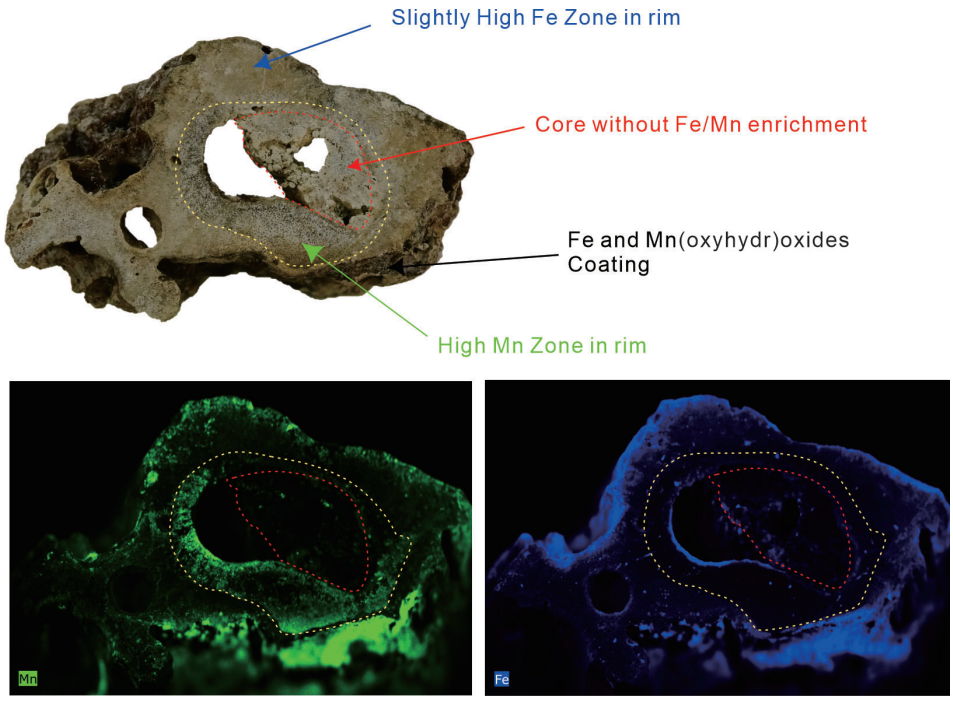

FIGURE 8
Fe and Mn scanning map of sample R3 obtained by high-resolution X-ray fluorescence (μXRF). The upper photograph shows the distribution of Fe/Mn elements on the fresh surface of the hand specimen. The bottom photographs show the scanning results of Mn (bottom left) and Fe (bottom right) elements on the fresh surface. The zoned distribution of Fe and Mn content is recognized (yellow dashed line). The coating on the outer and inner surfaces of the carbonates reveals both high Fe and Mn content. The core (red dashed line) does not reveal obvious Fe or Mn enrichment.

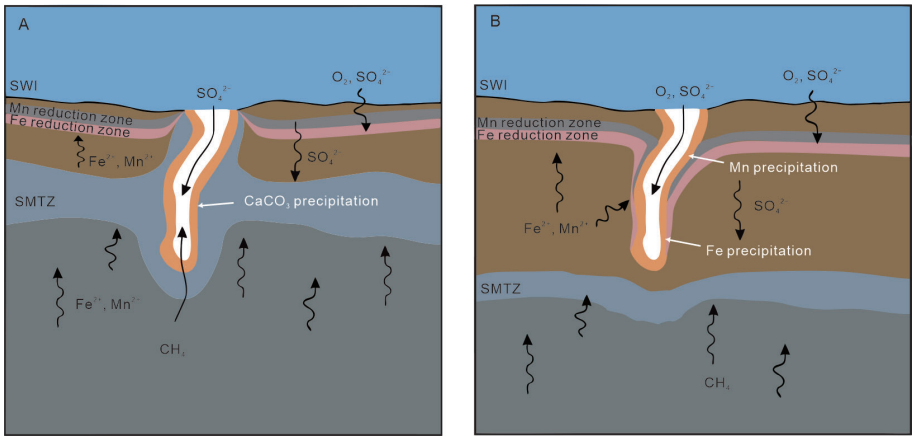

FIGURE 9
The proposed schematic diagram for the precipitation of the studied tubular carbonates (modified after Zwicker et al., 2015). **(A)** Tubular carbonate precipitates during relatively high seep flux. **(B)** Sulfate and methane transition zone (SMTZ) and Fe/Mn reduction zone migrated downward when flux decreased, facilitating Fe/Mn (oxyhydr)oxides to precipitate in the rims.

carbonates would be rich in Fe or Mn (oxyhydr)oxides, while the cores are not.

The morphology of tubular carbonates and/or the long-term interval between the seepage stages, as mentioned above, could facilitate the accumulation of Fe or Mn (oxyhydr)oxides. A similar scenario could occur in modern or ancient seep systems, although such high Fe or Mn (oxyhydr)oxides have not been widely recognized in methane-derived carbonates. The average Fe/Al ratio in the surface sediments in the Shenhu area is 0.52 (Zhao et al., 2009), which is slightly higher than that of the upper continental crust (0.44) and PAAS (0.45) (McLennan, 2001). However, compared to the sediments in other basins where methane-derived carbonate was recovered, such as the Krishna–Godavari sediments ($Fe/Al_{average}$: 0.8, Mazumdar et al., 2015) and the Campos Basin sediments (Fe/Al ratio > 1, Rezende et al., 2002), the ratio in the surface sediments in the Shenhu area is not significantly high. To date, few studies have focused on the Fe or Mn (oxyhydr)oxides in cold seep sediments and methane-derived carbonates. More attention to Fe or Mn cycles in methane seepage systems, especially where tubular carbonate occurs, is needed to settle this question.

Conclusion

Petrography, carbon and oxygen isotope compositions, and trace element contents of the tubular carbonates recovered in the Shenhu Sea Area in the northern South China Sea were investigated to reconstruct their formation environment and redox conditions. Moderately negative $\delta^{13}C$ values of the carbonates indicate a mixed carbon origin of biogenic and thermogenic methane. The low $\delta^{18}O$ values reflect an ^{18}O-depleted pore fluid, possibly induced by gas hydrate formation. The rims of carbonates R1 and R2 (group 1) are mainly composed of HMC and yield high Fe contents, while those of carbonates R3 and R4 (group 2) are mainly composed of aragonite and reveal high Mn contents. The positive relationship between Mo_{EF} and other enrichment factors of trace elements (W_{EF}, Co_{EF}, and Cr_{EF}) in the HMC rims with Fe enrichment (group 1) indicates Fe (oxyhydr)oxide enrichment. The positive relationship between Mo_{EF} and Mn/Al in the aragonite rims with Mn enrichment (group 2) reflects Mn (oxyhydr)oxide enrichment. The concurrent presence of Fe and Mn (oxyhydr)oxides on the outer and inner surfaces of the tubular carbonates and the absence of Fe or Mn enrichment in the cores of the tubular carbonates suggest that the Fe/Mn (oxyhydr)oxides in the rims did not precipitate during exposure in bottom seawater. The occurrence of dissolution textures in the rims favors the presence of episodic oxic conditions, which could facilitate Fe^{2+}/Mn^{2+} oxidation. The Fe^{2+} and Mn^{2+} could be transferred from underlying reducing sediments. Our results emphasize the complexity of the archives in seep carbonates. Similar processes and scenarios may apply to ancient seep systems that contain tubular carbonates or that show high seepage intensity. Our study provides new insights into the records in episodic oxic conditions in seep systems.

Data availability statement

The original contributions presented in the study are included in the article/Supplementary Material. Further inquiries can be directed to the corresponding author.

Author contributions

Conceptualization: QL and HH. Methodology: HH. Formal analysis: HH, YD, XX, and JF. Investigation: HH. Resources: QL. Data curation: QL. Writing—original draft preparation: QL, HH, XW, SG, and DF. Writing—review and editing: QL, HH, XW, and SG. Visualization: HH. Supervision: QL. Project administration: QL. Funding acquisition: QL, HH, and XX. All authors contributed to the article and approved the submitted version.

Funding

This work was supported by the Guangdong Basic and Applied Basic Research Foundation (Nos. 2019B030302004, 20201910240000691), the China Postdoctoral Science Foundation (No. 2021M703295), the National Natural Science Foundation of China (No. 41906076), and the Marine Geological Survey Program of China Geological Survey (DD20221706).

Acknowledgments

The authors express their sincere gratitude to the crews and participants of the *Haiyang-4* for their assistance in collecting, processing, and shipping the samples. The comments of Prof. Harald Strauss, Dr. Claudio Argentino, and another anonymous reviewer helped to improve this article.

Conflict of interest

The authors declare that the research was conducted in the absence of any commercial or financial relationships that could be construed as a potential conflict of interest.

Publisher's note

Supplementary material

The Supplementary Material for this article can be found online at: https://www.frontiersin.org/articles/10.3389/fmars.2022.945908/full#supplementary-material

References

Akintomide, O. A., Adebayo, S., Horn, J. D., Kelly, R. P., and Johannesson, K. H. (2021). Geochemistry of the redox-sensitive trace elements molybdenum, tungsten, and rhenium in the euxinic porewaters and bottom sediments of the pettaquamscutt river estuary, Rhode island. *Chem. Geol.* 584, 120499. doi: 10.1016/j.chemgeo.2021.120499

Algeo, T. J., and Tribovillard, N. (2009). Environmental analysis of paleoceanographic systems based on molybdenum-uranium covariation. *Chem. Geol.* 268, 211–225. doi: 10.1016/j.chemgeo.2009.09.001.

Aloisi, G., Pierre, C., Rouchy, J. M., Foucher, J. P., and Woodside, J. (2000). Methane-related authigenic carbonates of Eastern Mediterranean Sea mud volcanoes and their possible relation to gas hydrate estabilization. earth planet. *Sci. Lett.* 184, 321–338. doi: 10.1016/S0012-821X(00)00322-8

Argentino, C., Lugli, F., Cipriani, A., Conti, S., and Fontana, D. (2019). A deep fluid source of radiogenic Sr and highly dynamic seepage conditions recorded in Miocene seep carbonates of the northern Apennines (Italy). *Chem. Geol.* 522, 135–147. doi: 10.1016/j.chemgeo.2019.05.029

Bayon, G., Pierre, C., Etoubleau, J., Voisset, M., Cauquil, E., Marsset, T., et al. (2007). Sr/Ca and Mg/Ca ratios in Niger Delta sediments: Implications for authigenic carbonate genesis in cold seep environments. *Mar. Geol.* 241, 93–109. doi: 10.1016/j.margeo.2007.03.007

Bayon, G., Birot, D., Ruffine, L., Caprais, J.-C., Ponzevera, E., Bollinger, C., et al. (2011). Evidence for intense REE scavenging at cold seeps from the Niger delta margin. *Earth Planet. Sci. Lett.* 312, 443–452. doi: 10.1016/j.epsl.2011.10.008

Bayon, G., Dupré, S., Ponzevera, E., Etoubleau, J., Chéron, S., Pierre, C., et al. (2013). Formation of carbonate chimneys in the Mediterranean Sea linked to deep-water oxygen depletion. *Nat. Geosci.* 6, 755–760. doi: 10.1038/ngeo1888

Birgel, D., Feng, D., Roberts, H. H., and Peckmann, J. (2011). Changing redox conditions at cold seeps as revealed by authigenic carbonates from alaminos canyon, northern gulf of Mexico. *Chem. Geol.* 285, 82–96. doi: 10.1016/j.chemgeo.2011.03.004

Boetius, A., Ravenschlag, K., Schubert, C. J., Rickert, D., Widdel, F., Gieseke, A., et al. (2000). A marine microbial consortium apparently mediating anaerobic oxidation of methane. *Nature* 407, 623–626. doi: 10.1038/35036572

Boetius, A., and Wenzhöfer, F. (2013). Seafloor oxygen consumption fuelled by methane from cold seeps. *Nat. Geosci.* 6, 725–734. doi: 10.1038/ngeo1926

Bohrmann, G., Greinert, J., Suess, E., and Torres, M. (1998). Authigenic carbonates from the cascadia subduction zone and their relation to gas hydrate stability. *Geology* 26, 647–650. doi: 10.1130/0091-7613(1998)026<0647:ACFTCS>2.3.CO;2

Cai, W.-J., Chen, F., Powell, E. N., Walker, S. E., Parsons-Hubbard, K. M., Staff, G. M., et al. (2006). Preferential dissolution of carbonate shells driven by petroleum seep activity in the gulf of Mexico. *Earth Planet. Sci. Lett.* 248, 227–243. doi: 10.1016/j.epsl.2006.05.020

Campbell, K. A. (2006). Hydrocarbon seep and hydrothermal vent paleoenvironments and paleontology: Past developments and future research directions. *Palaeogeogr. Palaeoclimatol. Palaeoecol.* 232, 362–407. doi: 10.1016/j.palaeo.2005.06.018

Campbell, K. A., Francis, D. A., Collins, M., Gregory, M. R., Nelson, C. S., Greinert, J., et al. (2008). Hydrocarbon seep-carbonates of a Miocene forearc (East coast basin), north island, new Zealand. *Sediment. Geol.* 204, 83–105. doi: 10.1016/j.sedgeo.2008.01.002

Clark, J. F., Washburn, L., and Schwager Emery, K. (2010). Variability of gas composition and flux intensity in natural marine hydrocarbon seeps. *Geo-Marine Lett.* 30, 379–388. doi: 10.1007/s00367-009-0167-1

Dickens, G. R., O'Neil, J. R., Rea, D. K., and Owen, R. M. (1995). Dissociation of oceanic methane hydrate as a cause of the carbon isotope excursion at the end of the Paleocene. *Paleoceanography* 10, 965–971. doi: 10.1029/95PA02087

Feng, D., Chen, D., and Peckmann, J. (2009). Rare earth elements in seep carbonates as tracers of variable redox conditions at ancient hydrocarbon seeps. *Terra Nov.* 21, 49–56. doi: 10.1111/j.1365-3121.2008.00855.x

Feng, D., Roberts, H. H., Joye, S. B., and Heydari, E. (2014). Formation of low-magnesium calcite at cold seeps in an aragonite sea. *Terra Nov.* 26, 150–156. doi: 10.1111/ter.12081.

Feng, D., Peng, Y., Bao, H., Peckmann, J., Roberts, H. H., and Chen, D. (2016). A carbonate-based proxy for sulfate-driven anaerobic oxidation of methane. *Geology* 44, 999–1002. doi: 10.1130/G38233.1

Feng, D., Qiu, J.-W., Hu, Y., Peckmann, J., Guan, H., Tong, H., et al. (2018). Cold seep systems in the south China Sea: An overview. *J. Asian Earth Sci.* 168, 3–16. doi: 10.1016/j.jseaes.2018.09.021

Goldsmith, J. R., Graf, D. L., and Heard, H. L. (1961). Lattice constants of the calcium-magnesium carbonates. *Am. Mineral.* 46, 453–457.

Gong, S., Hu, Y., Li, N., Feng, D., Liang, Q., Tong, H., et al. (2018). Environmental controls on sulfur isotopic compositions of sulfide minerals in seep carbonates from the south China Sea. *J. Asian Earth Sci.* 168, 96–105. doi: 10.1016/j.jseaes.2018.04.037

Granina, L., Müller, B., and Wehrli, B. (2004). Origin and dynamics of Fe and Mn sedimentary layers in Lake Baikal. *Chem. Geol.* 205, 55–72. doi: 10.1016/j.chemgeo.2003.12.018

Greinert, J., Bohrmann, G., and Suess, E. (2013). "Gas Hydrate-Associated Carbonates and Methane-Venting at Hydrate Ridge: Classification, Distribution, and Origin of Authigenic Lithologies," in *Natural Gas Hydrates: Occurrence, Distribution, and Detection: Occurrence, Distribution, and Detection*, 99–113. doi: 10.1029/GM124p0099

Gustafsson, J. P. (2003). Modelling molybdate and tungstate adsorption to ferrihydrite. *Chem. Geol.* 200, 105–115. doi: 10.1016/S0009-2541(03)00161-X

Helz, G. R., Bura-Nakić, E., Mikac, N., and Ciglenečki, I. (2011). New model for molybdenum behavior in euxinic waters. *Chem. Geol.* 284, 323–332. doi: 10.1016/0016-7037(96)00195-0

Helz, G. R., Miller, C. V., Charnock, J. M., Mosselmans, J. F. W., Pattrick, R. A. D., Garner, C. D., et al. (1996). Mechanism of molybdenum removal from the sea and its concentration in black shales: EXAFS evidence. *Geochim. Cosmochim. Acta* 60, 3631–3642. doi: 10.1016/j.chemgeo.2011.03.012

Helz, G. R. (2022). The Re/Mo redox proxy reconsidered. *Geochim. Cosmochim. Acta* 317, 507–522. doi: 10.1016/j.gca.2021.10.029.

Himmler, T., Brinkmann, F., Bohrmann, G., and Peckmann, J. (2011). Corrosion patterns of seep-carbonates from the eastern Mediterranean Sea. *Terra Nov.* 23, 206–212. doi: 10.1111/j.1365-3121.2011.01000.x

Hinrichs, K.-U., Hayes, J. M., Sylva, S. P., Brewer, P. G., and DeLong, E. F. (1999). Methane-consuming archaebacteria in marine sediments. *Nature* 398, 802–805. doi: 10.1038/19751

Hovland, M., Talbot, M. R., Qvale, H., Olaussen, S., and Aasberg, L. (1987). Methane-related carbonate cements in pockmarks of the north Sea. *J. Sediment. Res.* 57, 881–892. doi: 10.1306/212f8c92-2b24-11d7-8648000102c1865d

Hu, Y., Feng, D., Peckmann, J., Roberts, H. H., and Chen, D. (2014). New insights into cerium anomalies and mechanisms of trace metal enrichment in authigenic carbonate from hydrocarbon seeps. *Chem. Geol.* 381, 55–66. doi: 10.1016/j.chemgeo.2014.05.014

Jørgensen, B. B., Böttcher, M. E., Lüschen, H., Neretin, L. N., and Volkov, I. I. (2004). Anaerobic methane oxidation and a deep H_2S sink generate isotopically heavy sulfides in black Sea sediments. *Geochim. Cosmochim. Acta* 68, 2095–2118. doi: 10.1016/j.gca.2003.07.017

Jin, M., Feng, D., Huang, K., Peckmann, J., Li, N., Huang, H., et al. (2021). Behavior of mg isotopes during precipitation of methane-derived carbonate: Evidence from tubular seep carbonates from the south China Sea. *Chem. Geol.* 567, 120101. doi: 10.1016/j.chemgeo.2021.120101

Joseph, C., Campbell, K. A., Torres, M. E., Martin, R. A., Pohlman, J. W., Riedel, M., et al. (2013). Methane-derived authigenic carbonates from modern and paleoseeps on the cascadia margin: Mechanisms of formation and diagenetic signals. *Palaeogeogr. Palaeoclimatol. Palaeoecol.* 390, 52–67. doi: 10.1016/j.palaeo.2013.01.012

Joshi, R. K., Mazumdar, A., Peketi, A., Ramamurty, P. B., Naik, B. G., Kocherla, M., et al. (2014). Gas hydrate destabilization and methane release events in the Krishna–godavari basin, bay of Bengal. *Mar. Pet. Geol.* 58, 476–489. doi: 10.1016/j.marpetgeo.2014.08.013

Kennett, J. P., Cannariato, K. G., Hendy, I. L., and Behl, R. J. (2000). Carbon isotopic evidence for methane hydrate instability during quaternary interstadials. *Science.* 288, 128–133. doi: 10.1126/science.288.5463.128

Kim, S.-T., and O'Neil, J. R. (1997). Equilibrium and nonequilibrium oxygen isotope effects in synthetic carbonates. *Geochim. Cosmochim. Acta* 61, 3461–3475. doi: 10.1016/S0016-7037(97)00169-5

Kim, S.-T., O'Neil, J. R., Hillaire-Marcel, C., and Mucci, A. (2007). Oxygen isotope fractionation between synthetic aragonite and water: Influence of temperature and Mg^{2+} concentration. *Geochim. Cosmochim. Acta* 71, 4704–4715. doi: 10.1016/j.gca.2007.04.019

Klaucke, I., Weinrebe, W., Petersen, C. J., and Bowden, D. (2010). Temporal variability of gas seeps offshore new Zealand: Multi-frequency geoacoustic imaging of the wairarapa area, hikurangi margin. *Mar. Geol.* 272, 49–58. doi: 10.1016/j.margeo.2009.02.009

Knab, N. J., Cragg, B. A., Hornibrook, E. R. C., Holmkvist, L., Pancost, R. D., Borowski, C., et al. (2009). Regulation of anaerobic methane oxidation in sediments of the black Sea. *Biogeosciences* 6, 1505–1518. doi: 10.5194/bg-6-1505-2009

Knittel, K., and Boetius, A. (2009). Anaerobic oxidation of methane: Progress with an unknown process. *Annu. Rev. Microbiol.* 63, 311–334. doi: 10.1146/annurev.micro.61.080706.093130

Lapham, L. L., Chanton, J. P., Martens, C. S., Sleeper, K., and Woolsey, J. R. (2008). Microbial activity in surficial sediments overlying acoustic wipeout zones at a gulf of Mexico cold seep. *Geochem. Geophys. Geosyst.* 9, Q06001. doi: 10.1029/2008GC001944

Lin, Z., Sun, X., Strauss, H., Eroglu, S., Böttcher, M. E., Lu, Y., et al. (2021). Molybdenum isotope composition of seep carbonates – constraints on sediment biogeochemistry in seepage environments. *Geochim. Cosmochim. Acta* 307, 56–71. doi: 10.1016/j.gca.2021.05.038

Liu, C., Ye, Y., Meng, Q., He, X., Lu, H., Zhang, J., et al. (2012). The characteristics of gas hydrates recovered from shenhu area in the south China Sea. *Mar. Geol.* 307, 22–27. doi: 10.1016/j.margeo.2012.03.004

Li, N., Yang, X., Peckmann, J., Zhou, Y., Wang, H., Chen, D., et al. (2021). Persistent oxygen depletion of bottom waters caused by methane seepage: Evidence from the south China Sea. *Ore Geol. Rev.* 129, 103949. doi: 10.1016/j.oregeorev.2020.103949

Luff, R., and Wallmann, K. (2003). Fluid flow, methane fluxes, carbonate precipitation and biogeochemical turnover in gas hydrate-bearing sediments at hydrate ridge, cascadia margin: Numerical modeling and mass balances. *Geochim. Cosmochim. Acta* 67, 3403–3421. doi: 10.1016/S0016-7037(03)00127-3

Lu, Y., Liu, Y., Sun, X., Lin, Z., Xu, L., Lu, H., et al. (2017). Intensity of methane seepage reflected by relative enrichment of heavy magnesium isotopes in authigenic carbonates: A case study from the south China Sea. *Deep Sea Res. Part I Oceanogr. Res. Pap.* 129, 10–21. doi: 10.1016/j.dsr.2017.09.005

Matsumoto, R. (1990). Vuggy carbonate crust formed by hydrocarbon seepage on the continental shelf of Baffin island, northeast Canada. *Geochem. J.* 24, 143–158. doi: 10.2343/geochemj.24.143

Mazumdar, A., Dewangan, P., Joäo, H. M., Peketi, A., Khosla, V. R., Kocherla, M., et al. (2009). Evidence of paleo-cold seep activity from the bay of Bengal, offshore India. *Geochem.Geophys. Geosyst.* 10, Q06005. doi: 10.1029/2008GC002337

Mazumdar, A., Joshi, R. K., Peketi, A., and Kocherla, M. (2011). Occurrence of faecal pellet-filled simple and composite burrows in cold seep carbonates: A glimpse of a complex benthic ecosystem. *Mar. Geol.* 289, 117–121. doi: 10.1016/j.margeo.2011.09.003

Mazumdar, A., Kocherla, M., Carvalho, M. A., Peketi, A., Joshi, R. K., Mahalaxmi, P., et al. (2015). Geochemical characterization of the Krishna–godavari and mahanadi offshore basin (Bay of Bengal) sediments: A comparative study of provenance. *Mar. Pet. Geol.* 60, 18–33. doi: 10.1016/j.marpetgeo.2014.09.005

McLennan, S. M. (2001). Relationships between the trace element composition of sedimentary rocks and upper continental crust. *Geochem. Geophys. Geosyst.* 2, 2000GC000109. doi: 10.1029/2000GC000109

Milkov, A. V. (2004). Global estimates of hydrate-bound gas in marine sediments: how much is really out there? *Earth-science Rev.* 66, 183–197. doi: 10.1016/j.earscirev.2003.11.002

Naehr, T. H., Stakes, D. S., and Moore, W. S. (2000). Mass wasting, ephemeral fluid flow, and barite deposition on the California continental margin. *Geology* 28, 315. doi: 10.1130/0091-7613(2000)28<315:MWEFFA>2.0.CO;2

Oppo, D., Capozzi, R., Picotti, V., and Ponza, A. (2015). A genetic model of hydrocarbon-derived carbonate chimneys in shelfal fine-grained sediments: The enza river field, northern Apennines (Italy). *Mar. Pet. Geol.* 66, 555–565. doi: 10.1016/j.marpetgeo.2015.03.002

Paull, C. K., Ussler, W.III, and Dillon, W. P. (1991). Is the extent of glaciation limited by marine gas-hydrates? *Geophys. Res. Lett.* 18, 432–434. doi: 10.1029/91GL00351

Peckmann, J., Birgel, D., and Kiel, S. (2009). Molecular fossils reveal fluid composition and flow intensity at a Cretaceous seep. *Geology* 37, 847–850. doi: 10.1130/G25658A.1

Peckmann, J., Reimer, A., Luth, U., Luth, C., Hansen, B., Heinicke, C., et al. (2001). Methane-derived carbonates and authigenic pyrite from the northwestern black Sea. *Mar. Geol.* 177, 129–150. doi: 10.1016/S0025-3227(01)00128-1

Peckmann, J., and Thiel, V. (2004). Carbon cycling at ancient methane-seeps. *Chem. Geol.* 205, 443–467. doi: 10.1016/j.chemgeo.2003.12.025

Phillips, R., and Xu, J. (2021). A critical review of molybdenum sequestration mechanisms under euxinic conditions: Implications for the precision of

molybdenum paleoredox proxies. *Earth-Science Rev.* 221, 103799. doi: 10.1016/j.earscirev.2021.103799

Reitner, J., Peckmann, J., Reimer, A., Schumann, G., and Thiel, V. (2005). Methane-derived carbonate build-ups and associated microbial communities at cold seeps on the lower Crimean shelf (Black Sea). *Facies* 51, 66–79. doi: 10.1007/s10347-005-0059-4

Rezende, C., Lacerda, L., Ovalle, A. R., Souza, C. M., Gobo, A. A., and Santos, D. (2002). The effect of an oil drilling operation on the trace metal concentrations in offshore bottom sediments of the Campos basin oil field, SE Brazil. *Mar. pollut. Bull.* 44, 680–684. doi: 10.1016/S0025-326X(02)00047-4

Ruppel, C. D., and Kessler, J. D. (2017). The interaction of climate change and methane hydrates. *Rev. Geophys.* 55, 126–168. doi: 10.1002/2016RG000534

Sato, H., Hayashi, K., Ogawa, Y., and Kawamura, K. (2012). Geochemistry of deep sea sediments at cold seep sites in the nankai trough: insights into the effect of anaerobic oxidation of methane. *Mar. Geol.* 323, 47–55. doi: 10.1016/j.margeo.2012.07.013

Schrag, D. P., Berner, R. A., Hoffman, P. F., and Halverson, G. P. (2002). On the initiation of a snowball earth. geochem. *Geophys. Geosyst.* 3, 1–21. doi: 10.1029/2001gc000219

Schulz, H. D. (2006) "Quantification of Early Diagenesis: Dissolved Constituents in Pore Water and Signals in the Solid Phase," in *Marine Geochemistry* (Berlin/Heidelberg: Springer-Verlag), 73–124. doi: 10.1007/3-540-32144-6_3.

Scott, C., and Lyons, T. W. (2012). Contrasting molybdenum cycling and isotopic properties in euxinic versus non-euxinic sediments and sedimentary rocks: Refining the paleoproxies. *Chem. Geol.* 324–325, 19–27. doi: 10.1016/j.chemgeo.2012.05.012

Shaw, T. J., Gieskes, J. M., and Jahnke, R. A. (1990). Early diagenesis in differing depositional environments: The response of transition metals in pore water. *Geochim. Cosmochim. Acta* 54, 1233–1246. doi: 10.1016/0016-7037(90)90149-F

Smrzka, D., Feng, D., Himmler, T., Zwicker, J., Hu, Y., Monien, P., et al. (2020). Trace elements in methane-seep carbonates: Potentials, limitations, and perspectives. *Earth-Science Rev.* 208, 103263. doi: 10.1016/j.earscirev.2020.103263

Smrzka, D., Zwicker, J., Bach, W., Feng, D., Himmler, T., Chen, D., et al. (2019). The behavior of trace elements in seawater, sedimentary pore water, and their incorporation into carbonate minerals: a review. *Facies* 65, 1–47. doi: 10.1007/s10347-019-0581-4

Solomon, E. A., Kastner, M., Jannasch, H., Robertson, G., and Weinstein, Y. (2008). Dynamic fluid flow and chemical fluxes associated with a seafloor gas hydrate deposit on the northern gulf of Mexico slope. *Earth Planet. Sci. Lett.* 270, 95–105. doi: 10.1016/j.epsl.2008.03.024

Stakes, D. S., Orange, D., Paduan, J. B., Salamy, K. A., and Maher, N. (1999). Cold-seeps and authigenic carbonate formation in Monterey bay, California. *Mar. Geol.* 159, 93–109. doi: 10.1016/S0025-3227(98)00200-X

Suess, E. (2018). ""Marine cold seeps: Background and recent advances,"," in *Hydrocarbons, oils and lipids: Diversity, origin, chemistry and fate* (Cham: Springer International Publishing), 1–21. doi: 10.1007/978-3-319-54529-5_27-1

Tarutani, T., Clayton, R. N., and Mayeda, T. K. (1969). The effect of polymorphism and magnesium substitution on oxygen isotope fractionation between calcium carbonate and water. *Geochim. Cosmochim. Acta* 33, 987–996. doi: 10.1016/0016-7037(69)90108-2

Tavormina, P. L., Ussler, W. III, and Orphan, V. J. (2008). Planktonic and sediment-associated aerobic methanotrophs in two seep systems along the north American margin. *Appl. Environ. Microbiol.* 74, 3985–3995. doi: 10.1128/AEM.00069-08

Taylor, S. R., and McLennan, S. M. (1985). *The Continental Crust: Its Composition and Evolution*. (Oxford: Blackwell). 312 pp.

Tong, H., Feng, D., Cheng, H., Yang, S., Wang, H., Min, A. G., et al. (2013). Authigenic carbonates from seeps on the northern continental slope of the south China Sea: New insights into fluid sources and geochronology. *Mar. Pet. Geol.* 43, 260–271. doi: 10.1016/j.marpetgeo.2013.01.011

Tryon, M. D., Brown, K. M., Torres, M. E., Tréhu, A. M., McManus, J., and Collier, R. W. (1999). Measurements of transience and downward fluid flow near episodic methane gas vents, hydrate ridge, cascadia. *Geology* 27, 1075–1078. doi: 10.1130/0091-7613(1999)027<1075:MOTADF>2.3.CO;2

Wang, J., Wu, S., Kong, X., Li, Q., Wang, J., and Ding, R. (2018). Geophysical characterization of a fine-grained gas hydrate reservoir in the shenhu area, northern south China Sea: Integration of seismic data and downhole logs. *Mar. Pet. Geol.* 92, 895–903. doi: 10.1016/j.marpetgeo.2018.03.020

Wei, J., Fang, Y., Lu, H., Lu, H., Lu, J., Liang, J., et al. (2018). Distribution and characteristics of natural gas hydrates in the shenhu Sea area, south China Sea. *Mar. Pet. Geol.* 98, 622–628. doi: 10.1016/j.marpetgeo.2018.07.028

Wei, J., Wu, T., Zhang, W., Deng, Y., Xie, R., Feng, J., et al. (2020). Deeply buried authigenic carbonates in the qiongdongnan basin, South China sea: Implications for ancient cold seep activities. *Minerals* 10, 1–19. doi: 10.3390/min10121135.

Wirsig, C., Kowsmann, R. O., Miller, D. J., de Oliveira Godoy, J. M., and Mangini, A. (2012). U/Th-dating and post-depositional alteration of a cold seep carbonate chimney from the Campos basin offshore Brazil. *Mar. Geol.* 329–331, 24–33. doi: 10.1016/j.margeo.2012.10.001

Wu, N., Yang, S., Zhang, H., Liang, J., Wang, H., Su, X., et al. (2008). Preliminary Discussion on Gas Hydrate Reservoir System of Shenhu Area , North Slope of South China Sea. in *Proceedings of the 6th International Conference on Gas Hydrates (ICGH 2008)*, 10–13. Vancouver, British Columbia, CANADA, July 6-10, 2008

Wu, N., Zhang, H., Yang, S., Zhang, G., Liang, J., Lu, J., et al. (2011). Gas hydrate system of shenhu area, northern south China Sea: Geochemical results. *J. Geol. Res.* 2011, 1–10. doi: 10.1155/2011/370298

Yang, K., Chu, F., Li, Ye, Zhang, W., Xu, D., Zhu, J. H., et al. (2014). No TitleImplication of methane seeps from sedimentary geochemical proxies (Sr/Ca & Mg/Ca) in the northern south China Sea (in Chinese). *J. Jilin Univ. (Earth Sci. Ed.)* 44, 469–479. doi: 10.13278/j.cnki.jjuese.201402106

Yang, K., Chu, F., Zhu, Z., Dong, Y., Yu, X., Zhang, W., et al. (2018). Formation of methane-derived carbonates during the last glacial period on the northern slope of the south China Sea. *J. Asian Earth Sci.* 168, 173–185. doi: 10.1016/j.jseaes.2018.01.022

Yang, J., Wang, X., Jin, J., Li, Y., Li, J., Qian, J., et al. (2017). The role of fluid migration in the occurrence of shallow gas and gas hydrates in the south of the pearl river mouth basin, south China Sea. *Interpretation* 5, SM1–SM11. doi: 10.1190/INT-2016-0197.1

Zhang, H. Q., Yang, S. X., Wu, N. Y., Su, X., Holland, M., Schultheiss, P., et al. (2007). Successful and surprising results for china's first gas hydrate drilling expedition. *Fire Ice Methane Hydrate Newsl.* 7, 6–9.

Zhao, Q. F., Gong, J. M., Chen, J. W., He, X. L., and Fu, S. Y. (2009). Characteristics of major elements and provenance analysis of surface sediments in the shenhu area, northern south China Sea. *Mar. Geol. Lett.* 25, 10–14. doi: 10.16028/j.1009-2722.2009.09.002

Zwicker, J., Smrzka, D., Gier, S., Goedert, J. L., and Peckmann, J. (2015). Mineralized conduits are part of the uppermost plumbing system of oligocene methane-seep deposits, Washington state (USA). *Mar. Pet. Geol.* 66, 616–630. doi: 10.1016/j.marpetgeo.2015.05.035